Motion in Magnetic Resonance
New Paradigms for Improved Clinical Diagnosis

Val M. Runge, MD, Johannes K. Richter, MD, and Johannes T. Heverhagen, MD, PhD

Abstract: Recent innovations in magnetic resonance, involving both hardware and software, that effectively deal with motion—whether inadvertent on the part of the patient or due to respiration and cardiac contraction—are reviewed, emphasizing major current advances. New technology involving motion sensing (kinetic, respiratory, and beat) is enabling simpler, faster, and more robust monitoring of the sources of motion. This information is being integrated, with new innovative imaging approaches, to effectively manage motion and its impact on image quality. Additional impact has been made by the use of compressed sensing and simultaneous multislice imaging, with these techniques maturing and being adopted to decrease scan time and thus the effect of motion. Guidance in terms of clinical use for techniques that effectively combat motion is provided, focusing on enabling faster and improved clinical scans. Magnetic resonance imaging is on the cusp of a major new leap forward in terms of image quality and clinical utility enabled by these technological advances.

Key Words: motion, magnetic resonance imaging, image quality

(*Invest Radiol* 2019;00: 00–00)

Motion is the most common unanticipated event associated with a magnetic resonance (MR) examination.[1] Motion during an examination degrades the images, leads to otherwise unnecessary repeated scans, prolongs the examination, and, in these and many other ways, adds to costs in addition to impacting negatively the diagnostic quality of the examination. In one study, unanticipated events were encountered in 17% of all MR patient studies, with one quarter of these being motion.[1] Evaluating the cost only due to the time required for repeated pulse sequences (additional imaging, to replace those with substantial motion, which occurred in 20% of the examinations), revenue forgone was approximately $115,000 per scanner per year, as calculated in 2014 US dollars.[2] Problems due to patient motion remain as one of the last unsolved challenges to improving image quality and thus the diagnostic utility of MR. This becomes even more evident with the continuing improvement in achievable spatial resolution for clinical scanners, with problems due to motion accentuated in higher-resolution images.

In this review, multiple strategies are presented for routine clinical MR imaging to make the examination more robust relative to motion. These include state-of-the-art approaches toward head movement, respiratory sensing (for breath-hold and free-breathing examinations), scan techniques that are intrinsically robust to motion (such as recent extensions of VIBE—also known as LAVA and THRIVE—for T1-weighted 3-dimensional [3D] imaging), and heart motion (Pilot Tone [PT]). Two major recent developments are also reviewed, which can be used to substantially accelerate scans without a loss in diagnostic quality (and by making the scan shorter, lessen any potential impact of motion), specifically compressed sensing (CS) and simultaneous multislice (SMS) imaging.

Received for publication January 31, 2019; and accepted for publication, after revision, March 3, 2019.

From the Department of Diagnostic, Interventional and Pediatric Radiology, University Hospital of Bern, Inselspital, University of Bern, Bern, Switzerland.

Val M. Runge and Johannes K. Richter are co-first authors.

Conflicts of interest and sources of funding: Partial support was provided by an unrestricted educational grant from Siemens Healthineers.

The images illustrated in this review article were acquired on 1.5 T and 3 T Siemens clinical magnetic resonance systems.

The scans featured in the figures were acquired at 3 T, with the exception of those in Figures 12 and 16 which were acquired at 1.5 T.

Correspondence to: Val M. Runge, MD, Department of Diagnostic, Interventional and Pediatric Radiology, University Hospital of Bern, Inselspital, University of Bern, Freiburgstrasse 10, CH-3010 Bern, Switzerland.

ISSN: 0020-9996/19/0000–0000
DOI: 10.1097/RLI.0000000000000566

Kinetic Sensing (Prospective Motion Correction)

Using a highly accurate in-bore camera, movement of the head—specifically translational and rotational changes—can be detected with a high accuracy (0.1 mm for translation and 0.1 degree for rotation). Prospective motion correction can then be achieved in all axes for both translation and rotation by continuously updating the field of view during the scan acquisition (correcting for both in-plane and through-plane motion). Such real-time prospective motion correction potentially offers a substantial advantage when compared with past approaches. The latter include different k-space sampling schemes such as BLADE (also known as PROPELLER and MultiVane) and radial imaging (motion minimization techniques as opposed to prospective correction), which have been shown to improve the diagnostic quality of images and are in clinical use today.[3,4]

Prospective motion correction with the kinetic sensor necessitates currently the placement of a marker on the bridge of the nose, which is then tracked by a camera system. This information forms the basis for motion correction, with sensing and correction of motion performed in real time. The rate of tracking of the sensor is important, with current systems able to achieve a rate of 60 frames per seconds. In addition, as opposed to other techniques such as the use of navigator echoes, neither scan time nor image contrast is affected.

As might be expected from basic principles, such prospective motion correction is likely to have its greatest impact with high-resolution imaging. Such systems should ideally function both in patients with mild motion (Figs. 1, 2), which is very common in the clinical environment, and in those with marked motion (Figs. 3–5), which includes a more limited group of patients, for example, pediatrics and uncooperative subjects. In terms of implementation for specific pulse sequences, 3D MP-RAGE (also known as 3D-FGRE, 3D fast SPGR, and 3D-TFE; Figs. 1, 3) and 2-dimensional (2D) fast spin echo (FSE, including FLAIR, Figs. 2, 4, 5) at 3 T would thus be first priority. Clinical applicability is anticipated as well for other high-resolution head scans such as 3D SPACE (also known as CUBE and VISTA, Fig. 6) and time-of-flight MRA (Fig. 7). Seven Tesla will also likely benefit from this approach, with initial clinical evaluation in progress. However, the market impact at 7 T will be less, at least initially, due to low number of clinical systems.

The first research focusing on prospective motion correction using an external tracking system was published in 2006, and outlined the general framework for the approach used today.[5] Caveats that had to be overcome include false motion correction due to facial motion (such as frowning or squinting) and loss of marker visibility.[6] Recently shown images at 7 T using the kinetic sensor and prospective motion correction are among the highest, if not the highest, true spatial resolution (due to the lack of image degradation caused by subject motion) images of the brain in vivo ever achieved.[7]

Respiratory Sensing

An important recent innovation for clinical MR is the ability to monitor the respiratory cycle by means of a coil that is an intrinsic part

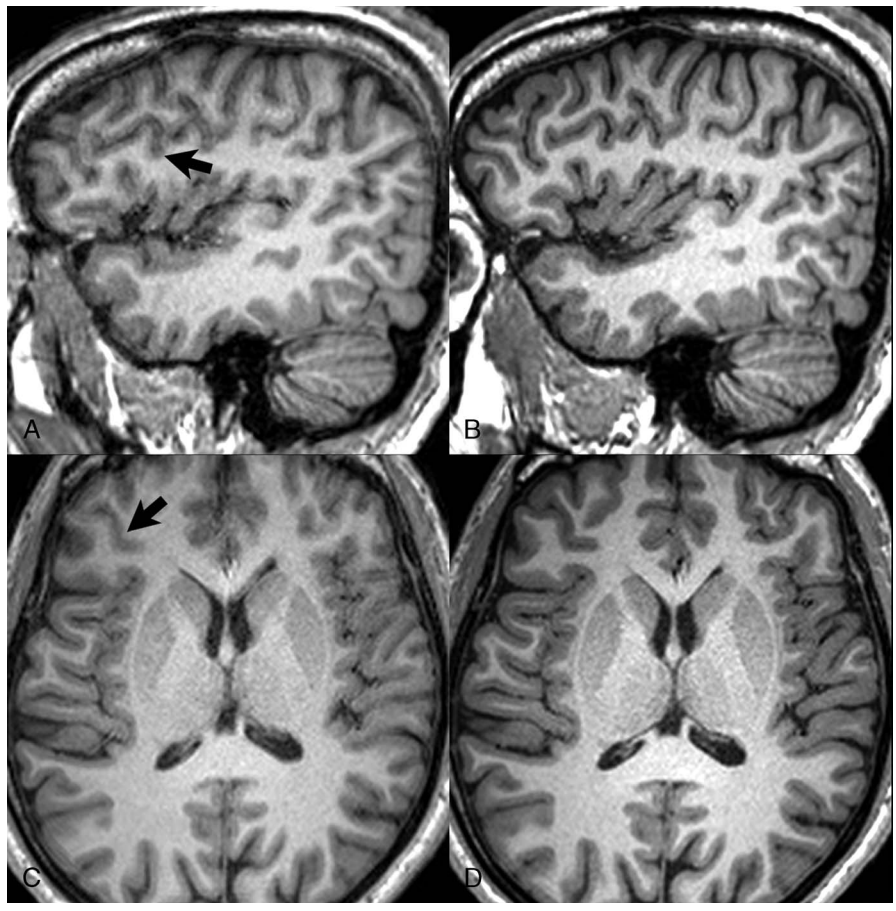

FIGURE 1. 3D MP-RAGE (A and C) without and (B and D) with implementation of the kinetic sensor for prospective motion correction, in a normal volunteer with mild motion. Note the mild blurring (black arrows) on (A and C) the images acquired without motion tracking, as well as the loss in gray-white matter differentiation, in particular anteriorly. B and D, Images acquired during the same mild motion but using the kinetic sensor exhibit a marked improvement in image quality, despite the relatively mild subject motion.

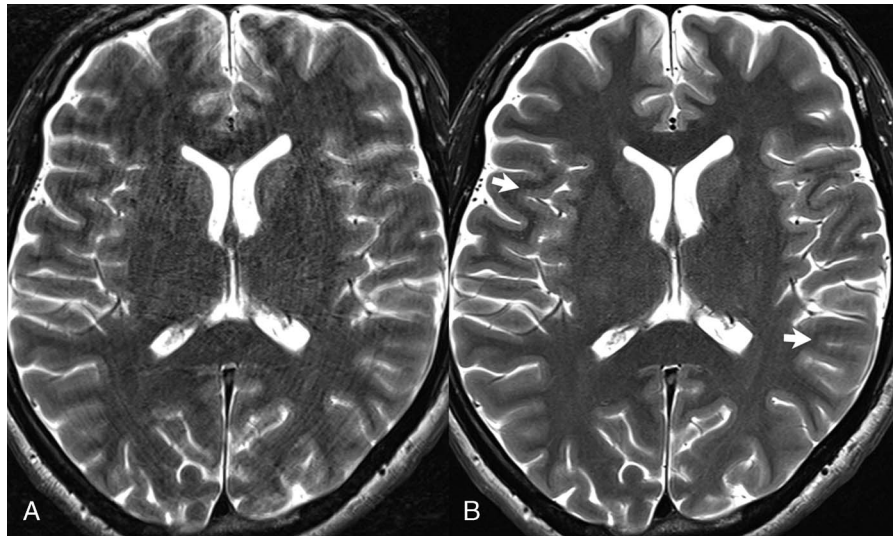

FIGURE 2. Image degradation (ghosting, blurring, loss of gray-white matter differentiation) due to mild motion in a normal volunteer, on (A) high-resolution T2-weighted fast spin echo imaging, with a marked improvement (B) using the kinetic sensor. Note the minimal residual ghosting (small white arrows) in the motion corrected image, superficial to the right insula and overlying the left parietal lobe.

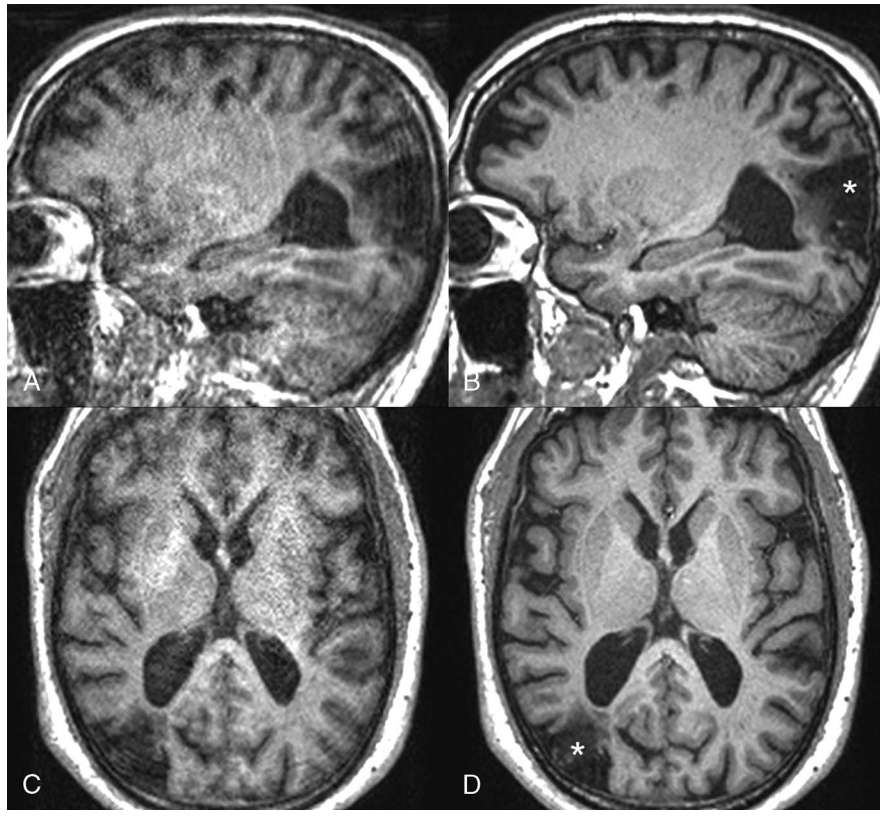

FIGURE 3. Prominent subject motion leading to substantial image degradation on sagittal and axial 3D MP-RAGE images (A and C), evaluation of a patient with a large, chronic, right-sided watershed infarct. Note the markedly improved depiction of this chronic infarct (asterisk), which demonstrates prominent cystic encephalomalacia (low signal intensity), on (B and D) scans acquired with prospective motion correction.

of the patient table, specifically within the spine coil. Respiratory monitoring (eg, by a bellows type device), and use of this signal for image acquisition and reconstruction, has a long history in MR, requiring setup time on the part of the technologist and was often not reliable, at least to the extent of its efficient use in scan acquisition.[8] Navigator echoes offer advantages and are commonly used today, but they require operator setup (being prone to misplacement) as well as time within the pulse sequence.[9]

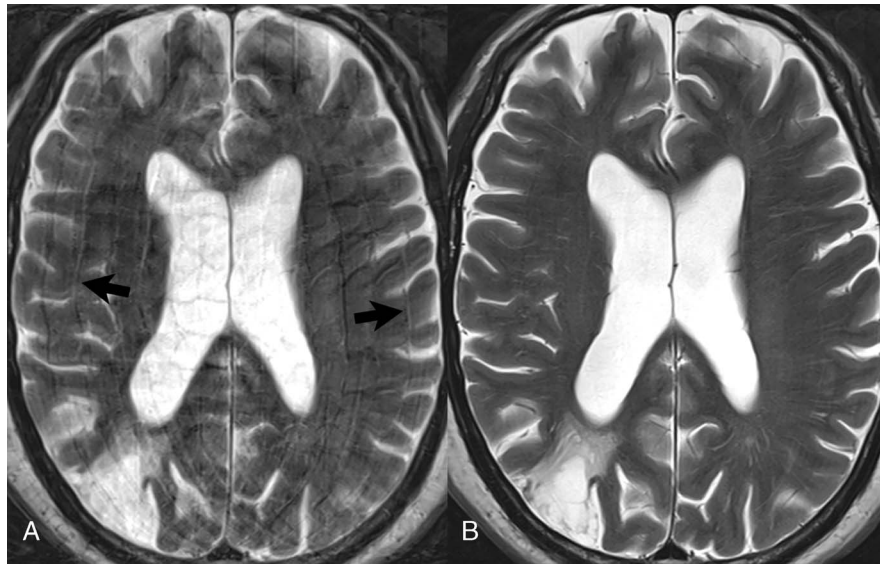

FIGURE 4. Improved depiction of a large watershed infarct in a patient with prominent motion (same subject as Figure 3) when comparing high-resolution T2-weighted fast spin echo scans acquired (A) without and (B) with prospective motion correction. Note the near complete elimination of ghosting artifacts in (B). These are prominent (arrows), tracking in the phase encoding direction (right to left), without motion correction (A).

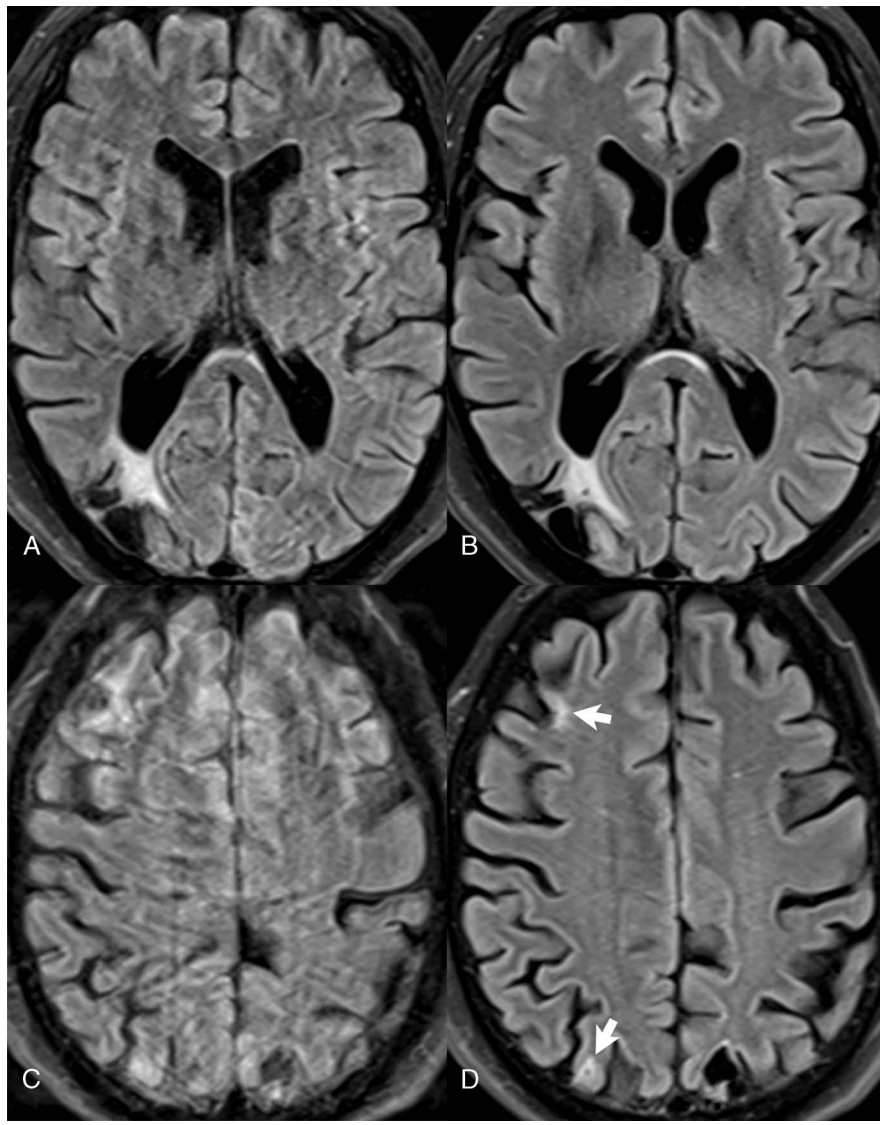

FIGURE 5. Efficacy of prospective motion correction in 2D FLAIR images, same patient as Figures 3 and 4. Two anatomic levels are shown (A and C) without and (B and D) with use of the kinetic sensor. On the lower level (A and B), there is cystic encephalomalacia and gliosis in the posterior MCA/PCA watershed region, better delineated with motion correction. On the upper level, mild gliosis is well seen both anteriorly and posteriorly in the watershed territory (arrows) with (D) motion correction, which is difficult to visualize on (C) the image without.

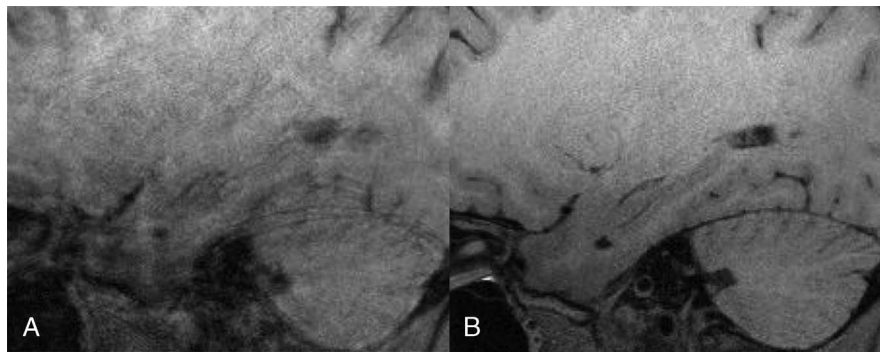

FIGURE 6. High-resolution 3D T1-weighted SPACE, in a moving subject (A) without and (B) with prospective motion correction. The scan time was 8 minutes in each instance, with a spatial resolution (voxel dimensions) of 0.56 mm^3. Motion artifacts (blurring and ghosting) make the image without correction nondiagnostic (Images courtesy of G. Laub).

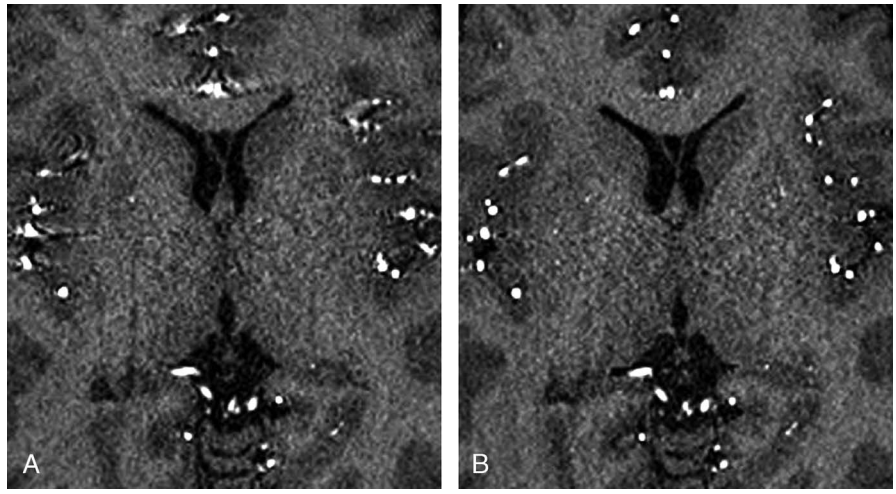

FIGURE 7. Illustration of the potential application of prospective motion correction in 3D time-of-flight (TOF) MRA. A GRE sequence was used in a TOF mode to create an MR angio-like image. Scan time was 3 minutes and 20 seconds for each image set (A) without and (B) with motion correction. The spatial resolution was 0.6 mm^3. Note the poor depiction of ACA, MCA, and PCA branches, seen in cross section, on (A) the image without motion correction, with substantial blurring and poor delineation of vessels (Images courtesy of G. Laub).

A summary of technical specifics follows for the respiratory sensor. This new technological advance requires no setup, is automatic, and provides a reliable, reproducible respiratory trace. An additional simple loop coil is integrated into the spine coil, which lies within the patient bed of the scanner. This coil, however, works at a different frequency, not the Larmor frequency (being specifically a 30-MHz transmit/receive coil), with changes therein thus able to be detected separately from the imaging signal. Respiration causes a change in the coil loading, which leads to current changes in the coil that can be detected and monitored (reflecting respiration). A small current is fed as input into the coil, and the resulting current output takes the form of the respiratory cycle, with slightly higher current during inhalation and lower during exhalation.

In reality, there are 2 such coils within the spine coil in the current implementation of this technology, because the coil for respiratory sensing needs to be placed over the diaphragm of the patient. One coil is located so that it lies automatically in the proper position for most individuals, regardless of height, when they are placed head first in the scanner. For feet-first investigations, including exceptionally tall or short individuals and pediatric patients, a second such coil is available, being located at the end of the spine coil. Detection of the respiratory signal, which occurs regardless of whether the patient is inside or outside of the bore, begins as soon as the patient lies down on the spine coil. In addition to its use in coordination with scan acquisition (eg, with respiratory-triggered scans), the respiratory sensor plays an important role for patient monitoring as well as providing a check for breath-hold scans in terms of the patient's ability to hold their breath for the duration of the scan.

Radial VIBE and Subsequent Developments

Radial VIBE (StarVIBE) is a 3D spoiled gradient-echo pulse sequence with a "stack of stars" radial readout and Cartesian phase encoding in the z direction of k-space. It is relatively motion robust and tolerates moderate undersampling. Its applicability was demonstrated early in liver imaging (Fig. 8).[10] Today it is used in many different body regions, including the orbits, head/neck, chest, and abdomen (including the bowel), and in pediatric imaging. When acquired with golden-angle radial sampling,[11] retrospective gating is possible and the sequence itself can provide the respiratory signal (self-gating). The utility of self-gated isotropic radial imaging has been demonstrated in the hepatobiliary phase after Gd-EOB-DTPA administration, providing multiplanar reformatted images with significantly superior image quality to conventional radial VIBE, using 40% data acceptance (self-gating).[12] As discussed in the subsequent section, this approach can also be used for motion correction on MR/PET.

To explain the evolution in pulse sequences in greater detail, with golden-angle sampling,[11] if the number of spokes is a Fibonacci number (a series of numbers in which each is the sum of the 2 preceding), then the angular k-space coverage of each image is almost uniform. This allows flexible adjustment of the temporal resolution. Interleaving of acquisition angles of temporal frames leads to temporal incoherence of undersampling artifacts, a necessary condition for CS. Using this approach, in combination with CS reconstruction, radial VIBE evolves to GRASP-VIBE (Fig. 9). This approach allows free-breathing contrast-enhanced multiphase liver MR, with flexible spatiotemporal resolution that can be tailored to clinical needs. The integrated self-gating option reduces the impact of respiratory motion. Thus, GRASP-VIBE has high clinical utility for the patient population with difficulty holding their breath (or cooperating with such instructions), thereby reducing failure rates for conventional dynamic abdominal MR.[13] Simultaneously, using this free-breathing approach, liver perfusion metrics (total plasma flow, portal venous flow, arterial perfusion fraction, mean transit time, and hepatocellular uptake rate—the latter assuming that Gd-EOB-DTPA was administered) can be acquired, without an additional contrast injection or requiring additional scan time.[14] GRASP-VIBE finds many applications as well outside the liver, due to its inherent robustness to motion, for example, in the female pelvis and prostate/rectum.[15]

GRASP-VIBE further evolves to XD-GRASP by adding respiratory motion-resolved reconstruction, with binning of data into different motion states instead of excluding data from certain motion states. By resolving respiratory motion retrospectively, image quality can be achieved superior to standard GRASP-VIBE.[16] Arterial phase reconstructions using this approach, with free-breathing, potentially achieve higher overall image quality compared with conventional breath-hold Cartesian acquisition, due in part to the limitations imposed by balancing temporal and spatial resolution with volumetric coverage accentuated by the transient dyspnea seen with Gd-EOB-DTPA.[17]

Similar to the evolution of reconstruction techniques for radial VIBE, corresponding CS variants have been developed for conventional VIBE with Cartesian k-space trajectory. For example, CS-VIBE is the Cartesian counterpart to the respiratory-gated GRASP-VIBE and XD-VIBE is the Cartesian counterpart to XD-GRASP. Relying on CS, both approaches allow dynamic, self-gated data acquisitions in

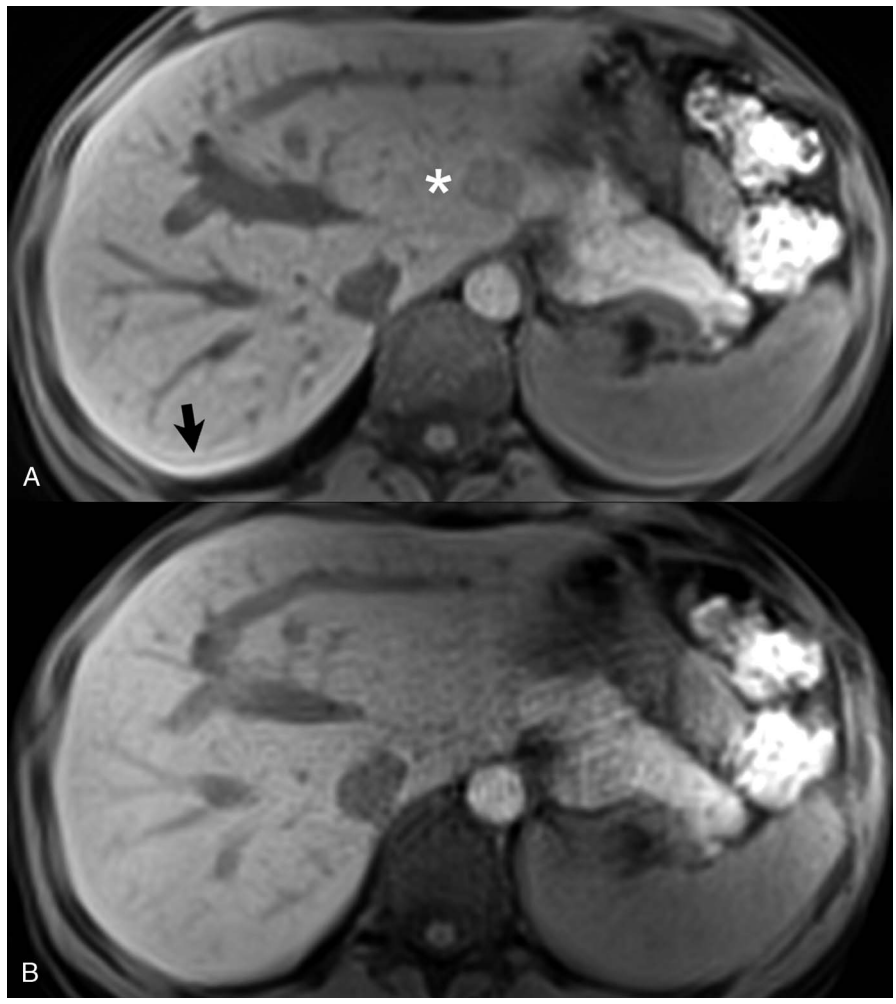

FIGURE 8. Radial acquisition by itself can effectively counter motion artifacts, with particular applicability in the head and neck region and pelvis. Its application is far broader, however, as illustrated by this comparison in the liver of a (A) conventional breath-hold VIBE scan to that of a (B) radial acquisition (StarVIBE). The scan time was 21 seconds in each instance, with the radial acquisition performed during shallow breathing. Note the aortic pulsation (asterisk) and truncation artifacts (arrow) in the conventional VIBE scan, with good image quality on the radial free-breathing examination. On the latter, streak artifacts, due to the short scan time restricting the number of radial views, are however present in the left upper quadrant, secondary to bowel motion.

free-breathing. Similar to their radial counterparts, CS-VIBE uses the data of the dominating motion state for a given gating acceptance providing a 3D plus time reconstruction. XD-VIBE bins the data into different motion states providing 3D plus time plus respiratory state reconstruction (Fig. 10). Clinical utility has been shown with these approaches as well.[18,19]

Respiratory Motion Correction for MR/PET

Integrated MR/PET systems with the possibility to simultaneously collect both data offer synergies by which information from each component modality can be used to improve image quality.[20] In particular, MR-based respiratory motion correction can be performed for the PET data. One current approach is to use radial imaging, which provides a self-gating signal. Data binning allows reconstruction of different respiratory phases. These data are then used to produce deformation fields and, with it, u-maps for each respiratory phase (ie, a motion model).[21] In more detail, MR self-gating is used to respiratory gate the MR and simultaneously acquired PET data. The motion model is used in a motion perceptive extension of the iterative ordered subset expectation maximization image reconstruction in PET to reconstruct the individual-gated data into a single motion compensated volume with preservation of SNR. PET localization and uptake quantification in the chest and abdomen can thus be improved, which is otherwise influenced by respiratory motion during the examination.

Compressed Sensing

Although not fully mature with still yet a wealth of undeveloped potential applications, CS has already had a major impact on the management of motion in MR. This has been achieved mainly on the basis of reducing scan time, and thus minimizing the effects of involuntary motion, respiration, and cardiac motion. Scan reconstruction times still remain long for more demanding applications (on the order of a few minutes). Although this is reasonable for clinical use, for most routine applications reconstruction times are below a minute. Further improvements in this area, given the continued advance in computer processing power, will make this rapidly a nonissue.

The CS variants of VIBE, including GRASP-VIBE, XD-GRASP, CS-VIBE, and XD-VIBE, have been discussed in detail earlier in this article, in particular with regard to their application for liver imaging. Of additional note is that liver perfusion can now be estimated from

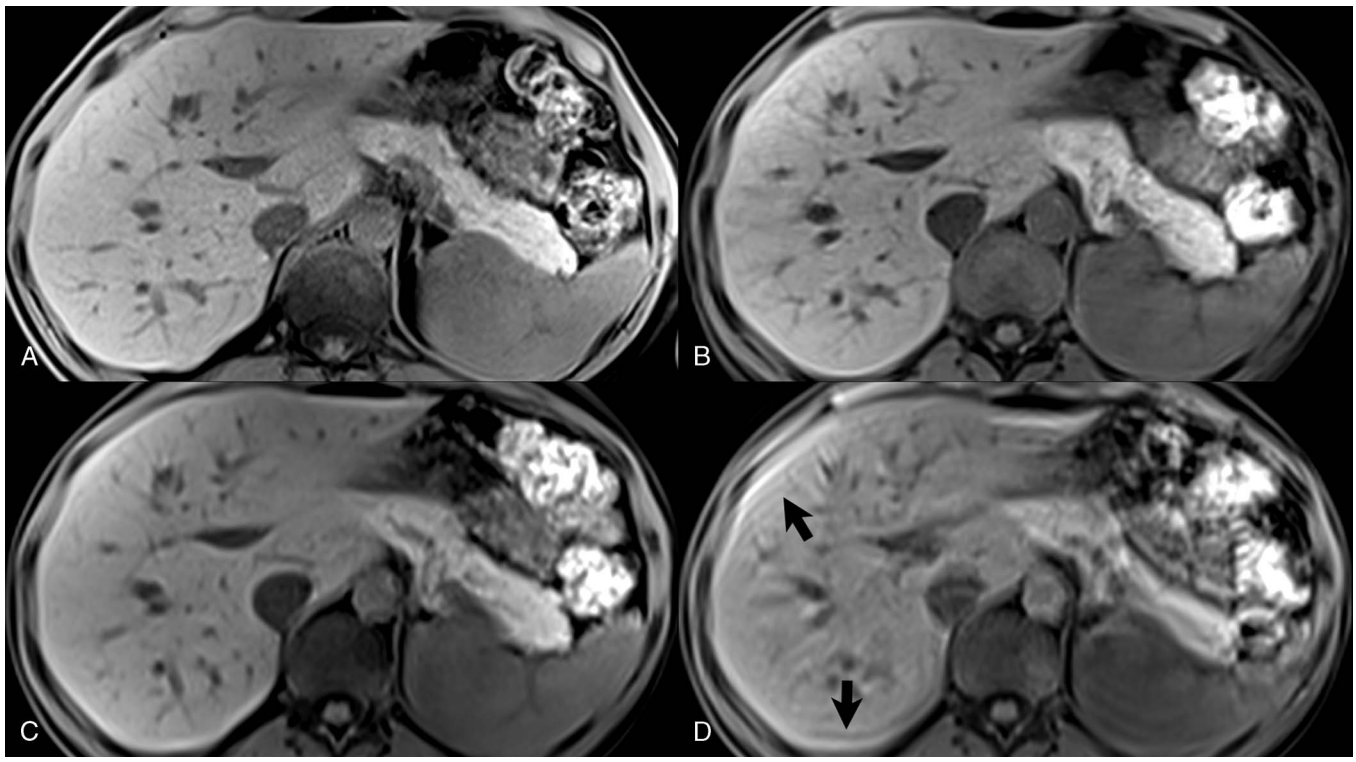

FIGURE 9. Optimizing strategies for liver imaging. A, Short breath-hold high-resolution VIBE is compared with (B) a lower resolution GRASP-VIBE (obtained during free-breathing), with comparisons as well to (C) a breath-hold VIBE scan with resolution close to that of the GRASP acquisition and (D) the same VIBE scan obtained without breath-holding. The latter scan is markedly degraded by respiratory motion artifacts (arrows). The slice thickness was 3 mm for all scans, with in-plane pixel resolutions of (A–C) 1.4 × 1.1, 1.5 × 1.5, and 2.0 × 1.5 mm^2. Scan times were 15, 22, and 12 seconds. B, GRASP-VIBE and (C) the lower voxel resolution breath-hold VIBE scan are of similar image quality. A, The high-resolution VIBE scan offers the best image quality (easily assessed in part by the depiction of vessels within the liver), although necessitating a breath-hold.

a free-breathing dynamic postcontrast scan, without the need for an additional contrast injection and without prolonging the examination time.[14] XD-GRASP, specifically, provides free-breathing motion-resolved reconstructions, as previously noted, leading to improved diagnostic quality multiphase images after intravenous gadolinium chelate administration.[16,22]

Compressed sensing magnetic resonance cholangiopancreatography (MRCP) is available at both 1.5 and 3 T, providing a major reduction in scan time.[23–25] Compressed sensing can be applied to the conventional sequence (resulting in one half to one third the scan time). Alternatively, at 3 T, diagnostic quality single breath-hold (16 seconds) MRCP scans are possible (Fig. 11). Given the difficulty in acquiring MRCP scans

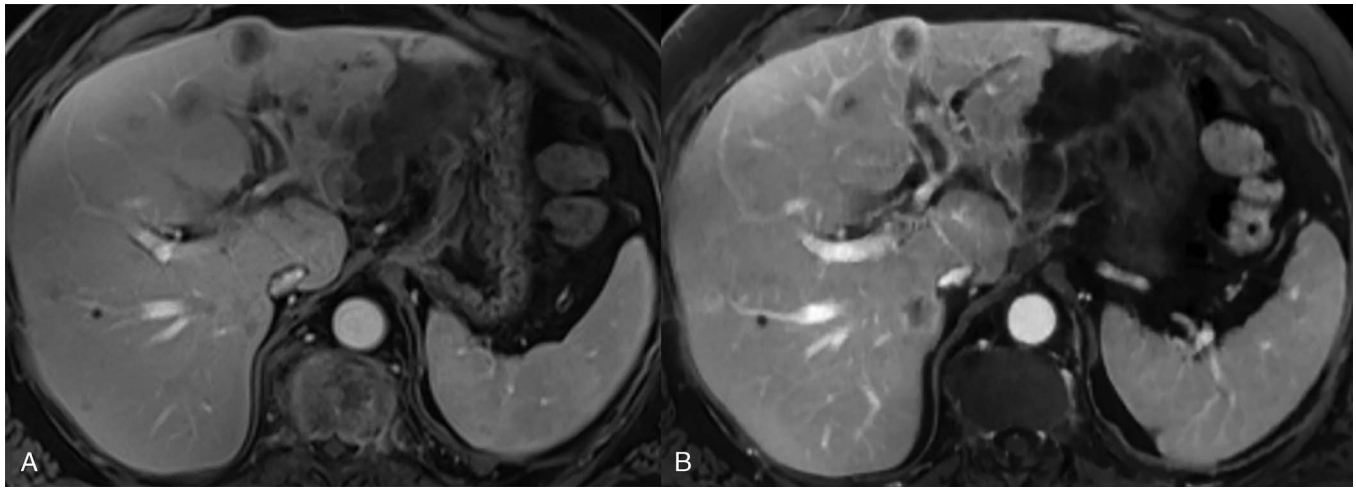

FIGURE 10. Venous phase images from (A) a standard breath-hold VIBE acquisition compared with (B) free-breathing XD-VIBE (both images are end-expiratory). Multiple liver metastases from colorectal cancer are visualized in both examinations. The Cartesian XD-VIBE acquisition enables motion state reconstruction, with excellent image quality, good temporal resolution, and accurate lesion detection (adapted with permission from *Invest Radiol* 2017;52:708–714).

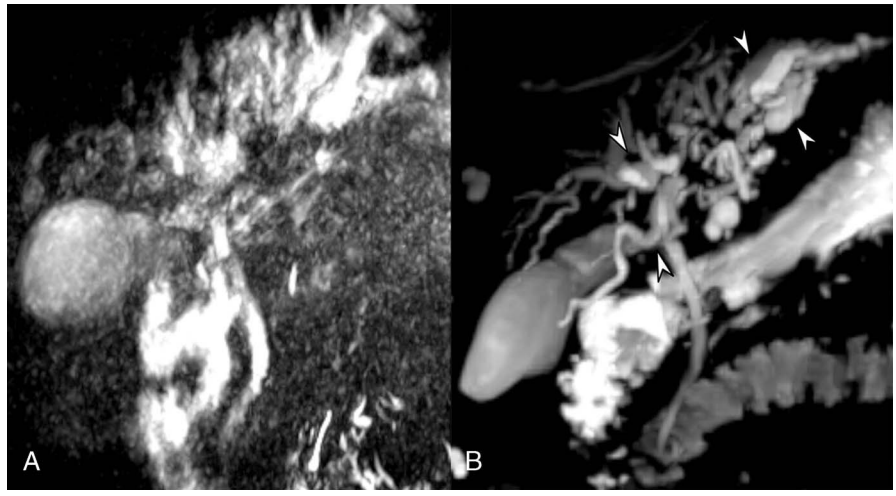

FIGURE 11. Three-dimensional MRCP scans acquired in a patient with a cholangiocarcinoma invading the portal hilum, comparison of (A) conventional and (B) breath-hold compressed sensing (CS) examinations. Scan times were 7 minutes on average (for the patient cohort evaluated) versus 16 seconds. The conventional examination is nondiagnostic due to motion. The breath-hold CS study well depicts the dilatation of the intrahepatic bile ducts (arrowheads) (adapted with permission from *Invest Radiol* 2017;52:612–619).

without substantial motion artifacts, and the length of such an examination, breath-hold CS MRCP examinations are very likely to become the criterion standard in this anatomic area in the future.

In cardiac imaging, CS already has made a significant impact. For 2 standard examinations, myocardial perfusion and CINE imaging, successful implementation of CS has been demonstrated. Single breath-hold 3D CINE imaging of the left ventricle with nearly isotropic resolution is feasible, with reformatting possible in arbitrary orientations and no statistically significant difference in ventricular function parameters when compared with values based on conventional 2D CINE, the latter requiring multiple breath-holds.[26] Acceleration has also been demonstrated with first-pass cardiac perfusion, for quantification of myocardial blood flow, allowing increased spatial coverage and higher spatial resolution.[27] Advances are being made as well in whole-heart coronary MRA with the use of CS, with decreased scan time a major objective.[28]

In musculoskeletal imaging, a major problem has been the artifact caused by surgically placed metal. Slice encoding for metal artifact correction (SEMAC) provided a major improvement, but was limited in clinical implementation due to long scan times. Initial studies with a CS version demonstrated high-quality metal artifact reduction, superior image quality to high bandwidth FSE imaging, and similar diagnostic quality to conventional lengthier (nonaccelerated) SEMAC.[29] In the last year, with further software evolution, clinically acceptable scan acquisition times, 2 to 6 minutes, have been demonstrated along with feasible reconstruction times.[30]

Beat Sensing

The next generation of heart motion sensors may well allow automatic capture of the cardiac cycle and replace the use of electrodes (electrocardiogram (ECG) monitoring), placement of the latter often being difficult and time consuming. The ECG signal is also prone to artifacts caused by activation of the gradients and the magnetohydrodynamic effect (particularly at higher field strengths). Coils are already available containing such a sensor, with sequences/applications still in development. Full-fledged implementation of such sensors is anticipated in the near future.

In the current concept, a local magnetic field generator is placed (embedded in an anterior coil), generating a PT that is modulated by changes in conductive geometry (including specifically heart motion).[31] This signal is subsequently detected with the nearby MR local receive coils. Coil combinations can be found that correlate well with the ECG and have also been shown to be stable and detectable during free-breathing, allowing acquisition of high-quality images of the heart (Fig. 12). The frequency used is just outside the MR signal band (64.4 MHz in initial work at 1.5 T). The PT design improves the robustness of cardiac acquisitions with regard to the gradients and placement of ECG leads. It also might allow for flexible trigger time point placement in the future. This single device, in a full implementation, could provide both cardiac and respiratory synchronization, as both motions influence the PT and can be observed. Implementation has been demonstrated for triggering cardiac sequences in normal volunteers at 1.5 T, with the acquired cine heart images (from prospective cardiac triggering) indistinguishable from that acquired using the ECG.[31] Pilot Tone prototypes have been implemented to date both on 1.5 and 3 T systems. Another potential advantage of PT navigation is that cardiac motion is measured directly (as opposed to observation of the electrical activity of the heart, which the ECG measures). In addition, unlike navigator echoes, PT navigation can be used with any scan sequence and does not necessitate the acquisition of additional navigator echoes.

Simultaneous Multislice

With SMS, multiple slices are excited simultaneously and then reconstructed individually. The latter involves the use of blipped

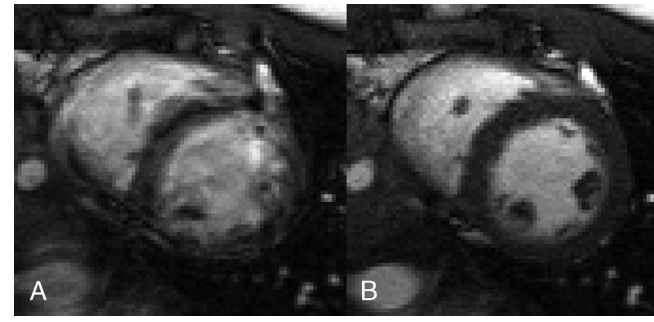

FIGURE 12. Midventricular short axis view of the heart comparing (A) an ECG mistriggered acquisition (using a synthetic trigger signal with an RR period of 1325 milliseconds) with (B) a Pilot Tone–triggered acquisition, both obtained in midsystole. Note the excellent visualization and delineation of the left ventricular wall and chamber in the Pilot Tone scan. Images were acquired at 1.5 T in a normal volunteer (Images courtesy of M. Bacher and P. Speier).

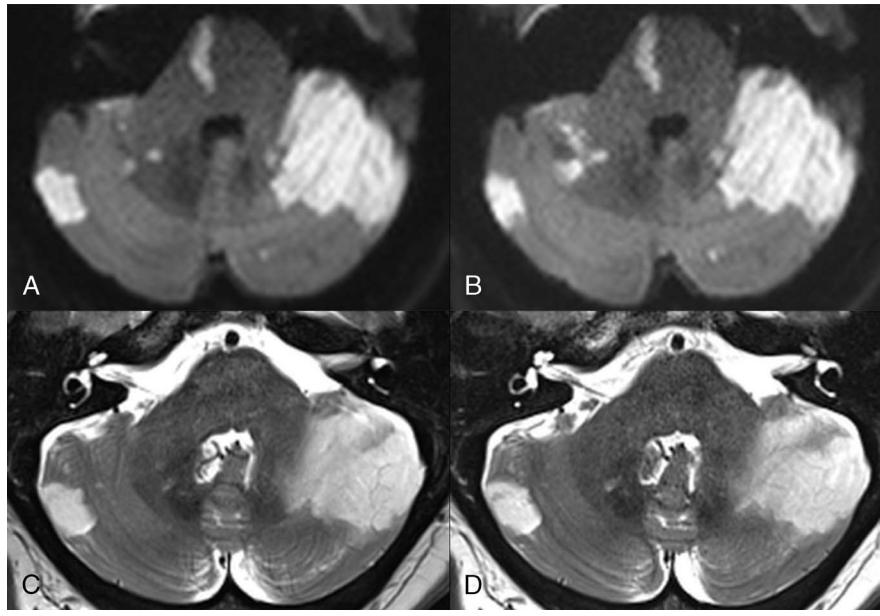

FIGURE 13. Multiple early subacute cerebellar infarcts, including one involving the right pons, visualized with high signal intensity on (A and B) DWI and (C and D) FSE T2-weighted scans—illustrating the utility of SMS. For the ss-echo-planar imaging (EPI) diffusion-weighted scans, the application of SMS (with 2× acceleration) reduced the scan time from (A) 1:23 to (B) 50 seconds. The decrease in scan time was achieved by reducing the TR from 6300 to 3500 milliseconds, with no loss in diagnostic quality. For the T2-weighted FSE comparison, use of a 3× acceleration combined with a reduction of the number of concatenations from (C) 3 to (D) 1 led to the scan time being reduced by a factor of 3.

CAIPIRINHA applied during the echo train (minimizing g-factor–related SNR loss), followed by slice GRAPPA-based unaliasing, and subsequently in-plane GRAPPA-based unaliasing.[32–34] For decreasing motion artifact, the focus of this review, current implementations exist for SMS in 2D multislice diffusion-weighted (echoplanar) and fast spin echo imaging (Fig. 13). Most clinical protocols today use an acceleration factor of 2 (although BOLD imaging protocols can easily reach an acceleration factor of 8), providing a reduction in scan time of approximately 40%.

Simultaneous excitation of multiple slices is achieved by using multiband pulses. Pulses for the different bands (slices) are phase-modulated and then summed to form a multiband radiofrequency excitation pulse. Critical in this process is optimization of the radiofrequency pulses with respect to energy deposition, with the latter one potential limitation of the SMS technique. For example, variable rate excitation (VERSE) can be applied to the 180-degree refocusing pulses. The use of blipped CAIPIRINHA is also critically important, as this enables a significant reduction in g-factor penalty. The g-factor is position-dependent and related to coil geometry, along with many other variables. It arises as a result of individual coil sensitivities being too similar. It can have a major negative impact on SNR, for example, in parallel imaging where the resultant SNR is dependent (and specifically inversely proportional) to the g-factor. Fortunately, in the clinical implementation of SMS, by use of blipped CAIPIRINHA, the g-factor penalty is essentially eliminated, for example, as shown by Setsompop for diffusion imaging from 32% to 1% for the case of 3-fold acceleration.[35]

Unfolding the slices (during scan reconstruction) requires for all slice GRAPPA-based SMS implementations the addition of a fast single-band reference scan, which necessitates additional time during the scan sequence. This leads, for example, with SMS 2, to the scan time not being quite half of that for a similar clinical scan without SMS. An additional important factor is the possibility of signal leakage between unaliased simultaneously acquired slices, which can create artifacts in the final images. These are mitigated by using a leak block algorithm.[36]

The difference between parallel imaging and SMS is important, yet often poorly understood. In parallel imaging, the number of acquired k-space lines is reduced by the acceleration factor R. Missing k-space lines are reconstructed using the coil sensitivity information. This results in an SNR loss proportional to the coil g factor and the square root of the acceleration factor. For SMS imaging with blipped CAIPIRINHA, the g-factor loss is minimized, and no additional reduction of acquired k-space lines takes place; hence, there is no SNR penalty proportional to the square root of the SMS factor.

It is also important to note that SMS benefits from higher channel-density coils. Thus, when given the choice between using a current 20 channel head/neck coil compared with a 64 channel head/neck coil (from the same manufacturer), the latter will provide higher SNR in the brain when using SMS and is the coil of choice.

For diffusion-weighted (echoplanar) scans, SMS allows the TR to be reduced while maintaining the number of slices, when compared with a conventional scan. For example, in Figure 13, the TR was reduced from (A) 6300 to (B) 3500 milliseconds. Changing the TR can, however, affect SNR and CNR, so depending upon the clinical protocol, the minimum TR (determined by the number of slices) may not be achievable.

Two-dimensional single-shot spin echo (ssSE) echo-planar imaging (EPI) is commonly used for diffusion-weighted imaging, both in brain and body applications. As conventionally acquired, this scan is highly time inefficient, due to the diffusion encoding being performed for the entire imaging volume for each single 2D slice excitation. Parallel imaging is typically performed, not for scan acceleration, but to shorten the EPI encoding period, reducing image distortion and blur. The scan time reduction for ssSE-EPI for the brain is, however, limited with the implementation of SMS, due to the scan often being quite short to begin with. For example, at 3 T, a typical scan time for 4-mm sections through the entire brain is only 1 minute and 23 seconds, with the implementation of SMS resulting in a decrease to 50 seconds (Figs. 13A, B). Due to the number of slices required for liver imaging (and the low SNR for body DWI), SMS can have a greater impact in this body region to shorten scan time (decreasing the effect of inadvertent patient

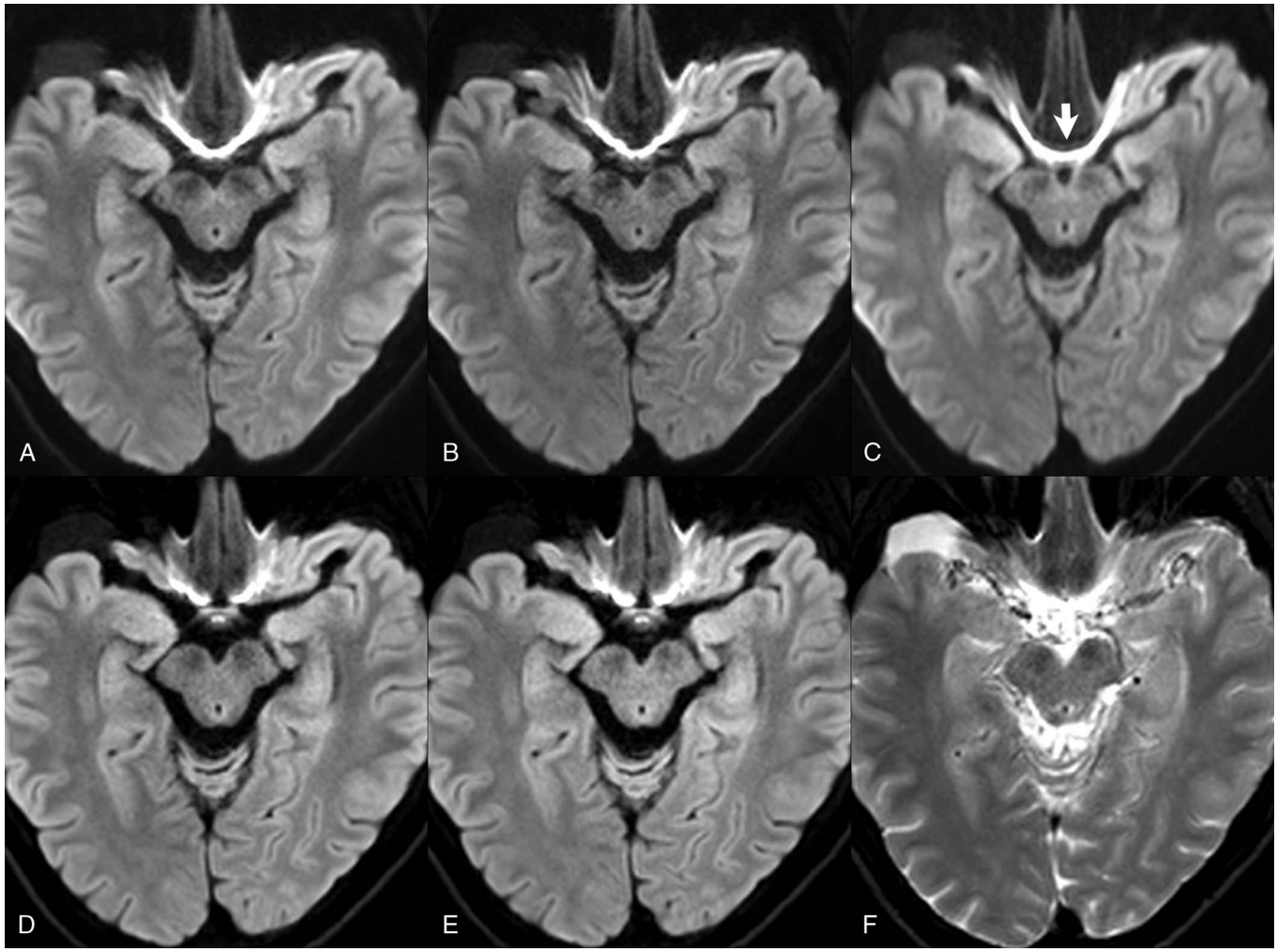

FIGURE 14. Scans comparing trace-weighted b 1000 (A and B) acoustic-noise–optimized DWI, (C) ss-EPI DWI, and (D and E) readout-segmented EPI DWI (RESOLVE), together with (F) the b 0 image corresponding to (E), in a patient with a small right middle cranial fossa arachnoid cyst. Applying SMS with a 2× acceleration, scan time could be reduced from (A) 4:35 to (B) 2 minutes and 39 seconds—specifically by lowering the TR from 6080 to 3160 milliseconds, allowing the quiet scan to be acquired within a reasonable time. Similarly, for the RESOLVE sequence scan time could be reduced from (D) 4 minutes and 20 seconds to (E) 2 minutes and 43 seconds by using 2× acceleration in combination with a reduction in TR from 5750 to 3800 milliseconds. Geometric distortion and bulk susceptibility artifacts (with that from the sphenoid sinus well seen, arrow) are least in the RESOLVE image and most in the ss-EPI DWI image.

motion).[37] A typical 3-mm scan through the entire liver at 3 T can be reduced from 4 minutes and 46 seconds with standard ssSE-EPI to 2 minutes and 54 seconds with SMS and an acceleration factor of 2. The impact of SMS on DWI of the prostate, enabling a 5-minute screening protocol for prostate cancer in patients with elevated prostate-specific antigen levels, has been recently demonstrated, with similar diagnostic performance of this abbreviated examination as compared with a full diagnostic multiparametric MR imaging session.[38]

Readout-segmented EPI (rs-EPI, RESOLVE) was developed subsequent to ss-EPI, with the advantages of reduced geometric distortion and blurring, which can be a substantial at 3 T with ss-EPI. The improved image quality is achieved by acquisition of subsets of k-space over several TRs rather than encoding the whole of k-space in a single shot. Visualization of areas prone to bulk susceptibility artifacts, for example in the brain close to the air-filled sinuses, is also markedly improved. An important limitation for rs-EPI is the longer scan time as compared with ss-EPI. Simultaneous multislice is used routinely today, in combination with a reduction in TR, for scan acceleration with rs-EPI.[39] The reduction in scan time, decreasing the chance of scan degradation due to inadvertent patient motion, is substantial (Fig. 14). Readout-segmented EPI is also used for acoustic noise–optimized DWI (reducing the noise of the scan for increased patient acceptance, Figs. 14A, B).[40] In this application, the echo spacing is increased (reducing the gradient noise), with a result that image distortion and bulk susceptibility artifacts will be greater (although much less than with ss-EPI; Fig. 14C, arrow). Important areas for the application of rs-EPI outside the brain include the spinal cord, head and neck cancer, and the breast (Fig. 15).

Simultaneous multislice techniques, initially applied to DWI, have now been extended as well to fast spin echo imaging. Simultaneous multislice can be applied with all tissue contrasts, specifically including proton density-, T1-, and T2-weighting. Anatomic areas of application for FSE SMS include the brain, neck, and, in particular, the musculoskeletal system (knee, hip, foot/ankle, hand/wrist). Examples of proton density weighted scans at 1.5 T, without and with SMS, in the knee and ankle are provided in Figure 16. Simultaneous multislice FSE is used for scan time reduction (one of the major ways to "manage" motion) in protocols that otherwise would need to use multiple concatenations (to get the required number of slices) or that need a large number of

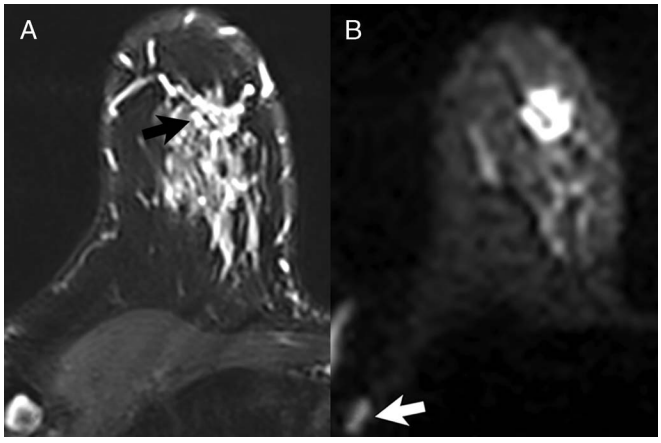

FIGURE 15. A spiculated mass lesion highly suspicious for malignancy is noted in the right breast of a 51-year-old woman on (A) T2-weighted and (B) rs-EPI DWI scans. The latter image series was acquired with 2× acceleration using SMS, leading to a scan time of 3 minutes and 17 seconds compared with a conventional acquisition, not shown, of 5 minutes and 52 seconds. A metastatic lymph node (arrow) is also noted in the right axilla (adapted with permission from *Invest Radiol* 2017;52:1–17).

slices (for example, axial long bone imaging). Its potential for accelerating knee imaging in particular is high, with similar quantitative and qualitative image quality demonstrated in a recent small clinical study evaluating the impact of approximately a 50% reduction in scan acquisition time using an acceleration factor of 2.[41] It also finds utility in trauma patients, to reduce the time the patient need be in the magnet (Fig. 17).

Although initially introduced for 3 T, SMS techniques have been extended to 1.5 T as well (Fig. 16). In regard to efficacy, specifically reducing scan time, there appears to be little difference between 1.5 and 3 T.

CONCLUSIONS

Motion can be managed in MR by sequence/technique selection and scan time reduction. Kinetic sensing is being developed for detection and prospective correction of head movement, with early results demonstrating a marked improvement in image quality, whether the motion be mild or more prominent. Respiratory sensing using an additional loop coil in the patient bed (operating at an independent frequency) has been introduced recently, offering an innovative, reliable solution to respiratory gating of scans, in addition to patient monitoring. Radial VIBE and subsequent VIBE variants, including GRASP-VIBE and XD-VIBE, offer motion robustness, the possibility of self-gating,

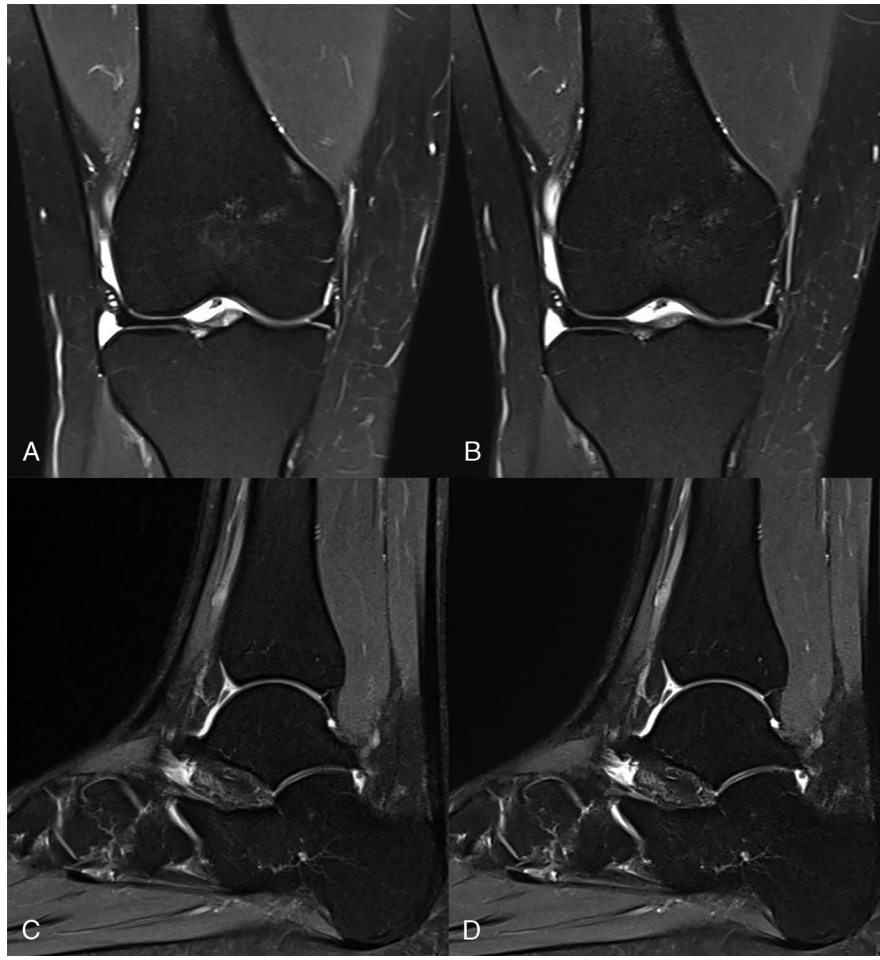

FIGURE 16. Proton density-weighted FSE images acquired at 1.5 T with fat suppression of (A and B) the knee in the coronal plane and (C and D) the ankle in the sagittal plane demonstrate mild joint effusions but are otherwise normal. Panels A and C were acquired with conventional technique, whereas (B and D) were acquired using a 2× acceleration with SMS. Image quality is equivalent. Scan times were (A and B) 3:20 versus 1 minutes and 51 seconds and (C and D) 2 minutes and 3 seconds versus 1 minutes and 24 seconds. The only change in scan parameters for the knee examination was a reduction in number of concatenations from 2 to 1, and for the ankle examination, a reduction in TR from 2800 to 2000 milliseconds.

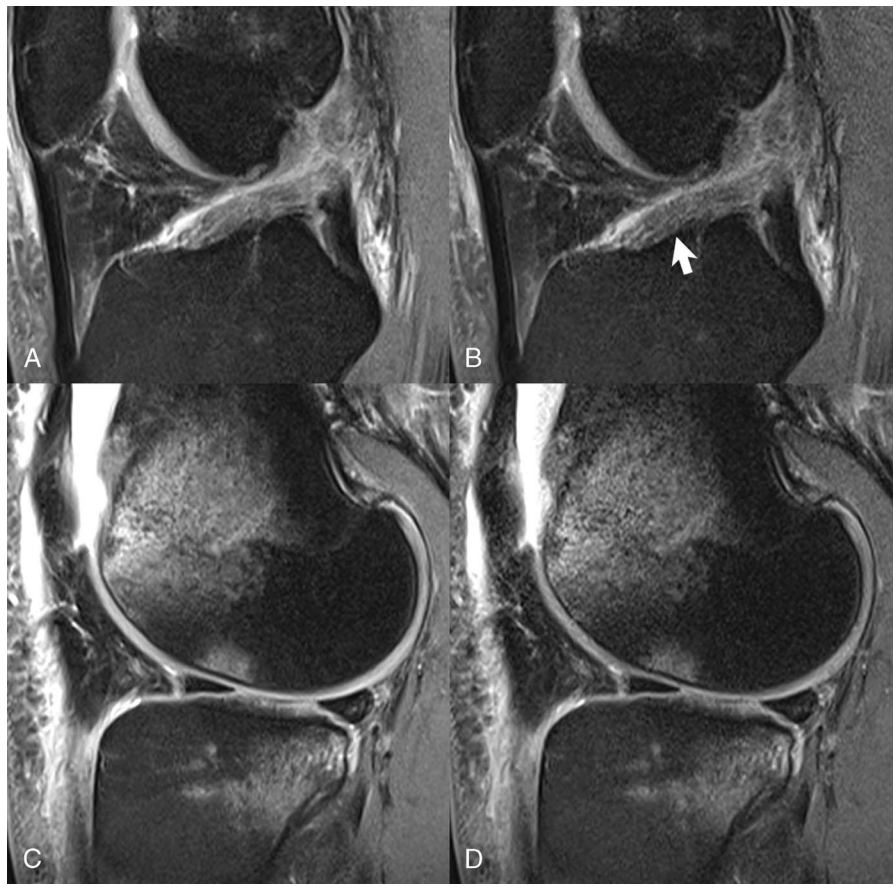

FIGURE 17. A ruptured ACL (arrow) with anterior displacement of the tibia relative to the femur is seen in this patient with a traumatic knee injury (due to a motorcycle accident). Multiple marrow contusions are also visualized, both in the distal femur and proximal tibia. Sagittal proton density-weighted scans (with fat suppression) are presented, acquired (A and C) without and (B and D) with SMS. A 2× acceleration was employed, leading to a scan time of only 1 minutes and 34 seconds for the images on the right, approximately half that of the scan without SMS. The depiction of pathology is equivalent (adapted with permission from *Invest Radiol* 2017;52:1–17).

free-breathing approaches, and non–breath-hold dynamic contrast-enhanced scans. Compressed sensing can be used to substantially reduce scan times, limiting inadvertent motion and the image degradation therein. Beat sensing, using hardware embedded in an anterior coil, is in early development and appears feasible, offering robust, direct detection of heart motion for cardiac imaging and removing the difficulties inherent with ECG placement and monitoring. Simultaneous multislice offers an effective means to combat potential motion, when used for a reduction in scan time. This is achieved with EPI scans (for diffusion weighting) by reducing the TR, and with FSE scans (for proton density, T1- and T2-weighting) in those situations where 2 or more concatenations would otherwise be required (for sufficient anatomic coverage). Most clinical applications to date feature an acceleration factor of 2, with a scan time reduction near but not reaching 50% due to the need for a reference scan. Together, these new paradigms advance clinical MR substantially in one of its last major challenges, which is effectively dealing with patient motion.

REFERENCES

1. Sadigh G, Applegate KE, Saindane AM. Prevalence of unanticipated events associated with MRI examinations: a benchmark for MRI quality, safety, and patient experience. *J Am Coll Radiol*. 2017;14:765–772.
2. Gumus K, Keating B, White N, et al. Comparison of optical and MR-based tracking. *Magn Reson Med*. 2015;74:894–902.
3. Wintersperger BJ, Runge VM, Biswas J, et al. Brain magnetic resonance imaging at 3 Tesla using BLADE compared with standard rectilinear data sampling. *Invest Radiol*. 2006;41:586–592.
4. Shin HJ, Kim MJ, Lee MJ, et al. Comparison of image quality between conventional VIBE and radial VIBE in free-breathing paediatric abdominal MRI. *Clin Radiol*. 2016;71:1044–1049.
5. Zaitsev M, Dold C, Sakas G, et al. Magnetic resonance imaging of freely moving objects: prospective real-time motion correction using an external optical motion tracking system. *Neuroimage*. 2006;31:1038–1050.
6. Singh A, Zahneisen B, Keating B, et al. Optical tracking with two markers for robust prospective motion correction for brain imaging. *MAGMA*. 2015;28:523–534.
7. Stucht D, Danishad KA, Schulze P, et al. Highest resolution in vivo human brain MRI using prospective motion correction. *PLoS One*. 2015;10:e0133921.
8. Runge VM, Clanton JA, Partain CL, et al. Respiratory gating in magnetic resonance imaging at 0.5 Tesla. *Radiology*. 1984;151:521–523.
9. Liu YL, Riederer SJ, Rossman PJ, et al. A monitoring, feedback, and triggering system for reproducible breath-hold MR imaging. *Magn Reson Med*. 1993;30:507–511.
10. Chandarana H, Block TK, Rosenkrantz AB, et al. Free-breathing radial 3D fat-suppressed T1-weighted gradient echo sequence: a viable alternative for contrast-enhanced liver imaging in patients unable to suspend respiration. *Invest Radiol*. 2011;46:648–653.
11. Winkelmann S, Schaeffter T, Koehler T, et al. An optimal radial profile order based on the Golden Ratio for time-resolved MRI. *IEEE Trans Med Imaging*. 2007;26:68–76.
12. Weiss J, Taron J, Othman AE, et al. Feasibility of self-gated isotropic radial late-phase MR imaging of the liver. *Eur Radiol*. 2017;27:985–994.

13. Chandarana H, Feng L, Block TK, et al. Free-breathing contrast-enhanced multiphase MRI of the liver using a combination of compressed sensing, parallel imaging, and golden-angle radial sampling. *Invest Radiol*. 2013;48:10–16.
14. Chandarana H, Block TK, Ream J, et al. Estimating liver perfusion from free-breathing continuously acquired dynamic gadolinium-ethoxybenzyl-diethylenetriamine pentaacetic acid-enhanced acquisition with compressed sensing reconstruction. *Invest Radiol*. 2015;50:88–94.
15. Attenberger UI, Liu J, Riffel P, et al. Quantitative perfusion analysis of the rectum using golden-angle radial sparse parallel magnetic resonance imaging: initial experience and comparison to time-resolved angiography with interleaved stochastic trajectories. *Invest Radiol*. 2017;52:715–724.
16. Chandarana H, Feng L, Ream J, et al. Respiratory motion-resolved compressed sensing reconstruction of free-breathing radial acquisition for dynamic liver magnetic resonance imaging. *Invest Radiol*. 2015;50:749–756.
17. Yoon JH, Lee JM, Yu MH, et al. Evaluation of transient motion during gadoxetic acid-enhanced multiphasic liver magnetic resonance imaging using free-breathing golden-angle radial sparse parallel magnetic resonance imaging. *Invest Radiol*. 2018;53:52–61.
18. Yoon JH, Yu MH, Chang W, et al. Clinical feasibility of free-breathing dynamic T1-weighted imaging with gadoxetic acid-enhanced liver magnetic resonance imaging using a combination of variable density sampling and compressed sensing. *Invest Radiol*. 2017;52:596–604.
19. Weiss J, Notohamiprodjo M, Taron J, et al. Continuous hepatic arterial multiphase magnetic resonance imaging during free-breathing. *Invest Radiol*. 2018;53:596–601.
20. Boada FE, Koesters T, Block KT, et al. Improved detection of small pulmonary nodules through simultaneous MR/PET imaging. *Magn Reson Imaging Clin N Am*. 2017;25:273–279.
21. Grimm R, Furst S, Souvatzoglou M, et al. Self-gated MRI motion modeling for respiratory motion compensation in integrated PET/MRI. *Med Image Anal*. 2015;19:110–120.
22. Feng L, Axel L, Chandarana H, et al. XD-GRASP: golden-angle radial MRI with reconstruction of extra motion-state dimensions using compressed sensing. *Magn Reson Med*. 2016;75:775–788.
23. Taron J, Weiss J, Notohamiprodjo M, et al. Acceleration of magnetic resonance cholangiopancreatography using compressed sensing at 1.5 and 3 T: a clinical feasibility study. *Invest Radiol*. 2018;53:681–688.
24. Yoon JH, Lee SM, Kang HJ, et al. Clinical feasibility of 3-dimensional magnetic resonance cholangiopancreatography using compressed sensing: comparison of image quality and diagnostic performance. *Invest Radiol*. 2017;52:612–619.
25. Zhu L, Wu X, Sun Z, et al. Compressed-sensing accelerated 3-dimensional magnetic resonance cholangiopancreatography: application in suspected pancreatic diseases. *Invest Radiol*. 2018;53:150–157.
26. Wetzl J, Schmidt M, Pontana F, et al. Single-breath-hold 3-D CINE imaging of the left ventricle using Cartesian sampling. *MAGMA*. 2018;31:19–31.
27. Naresh NK, Haji-Valizadeh H, Aouad PJ, et al. Accelerated, first-pass cardiac perfusion pulse sequence with radial k-space sampling, compressed sensing, and k-space weighted image contrast reconstruction tailored for visual analysis and quantification of myocardial blood flow. *Magn Reson Med*. 2019;81:2632–2643.
28. Bustin A, Ginami G, Cruz G, et al. Five-minute whole-heart coronary MRA with sub-millimeter isotropic resolution, 100% respiratory scan efficiency, and 3D-PROST reconstruction. *Magn Reson Med*. 2019;81:102–115.
29. Fritz J, Ahlawat S, Demehri S, et al. Compressed sensing SEMAC: 8-fold accelerated high resolution metal artifact reduction MRI of cobalt-chromium knee arthroplasty implants. *Invest Radiol*. 2016;51:666–676.
30. Jungmann PM, Bensler S, Zingg P, et al. Improved visualization of juxtaprosthetic tissue using metal artifact reduction magnetic resonance imaging: experimental and clinical optimization of compressed sensing SEMAC. *Invest Radiol*. 2019; 54:23–31.
31. Bacher M, Speier P, Bollenbeck J, et al. Pilot tone navigation enables contactless prospective cardiac triggering: initial volunteer results for prospective cine. *Proceedings of the 26th Annual Meeting of the ISMRM, #2960*. 2018. Available at: http://archive.ismrm.org/2018/2960.html. Accessed March 18, 2019.
32. Setsompop K, Gagoski BA, Polimeni JR, et al. Blipped-controlled aliasing in parallel imaging for simultaneous multislice echo planar imaging with reduced g-factor penalty. *Magn Reson Med*. 2012;67:1210–1224.
33. Barth M, Breuer F, Koopmans PJ, et al. Simultaneous multislice (SMS) imaging techniques. *Magn Reson Med*. 2016;75:63–81.
34. Runge VM, Richter JK, Heverhagen JT. Speed in clinical magnetic resonance. *Invest Radiol*. 2017;52:1–17.
35. Setsompop K, Cohen-Adad J, Gagoski BA, et al. Improving diffusion MRI using simultaneous multi-slice echo planar imaging. *Neuroimage*. 2012;63:569–580.
36. Cauley SF, Polimeni JR, Bhat H, et al. Interslice leakage artifact reduction technique for simultaneous multislice acquisitions. *Magn Reson Med*. 2014;72:93–102.
37. Taron J, Martirosian P, Schwenzer NF, et al. Scan time minimization in hepatic diffusion-weighted imaging: evaluation of the simultaneous multislice acceleration technique with different acceleration factors and gradient preparation schemes. *MAGMA*. 2016;29:739–749.
38. Weiss J, Martirosian P, Notohamiprodjo M, et al. Implementation of a 5-minute magnetic resonance imaging screening protocol for prostate cancer in men with elevated prostate-specific antigen before biopsy. *Invest Radiol*. 2018;53:186–190.
39. Frost R, Jezzard P, Douaud G, et al. Scan time reduction for readout-segmented EPI using simultaneous multislice acceleration: diffusion-weighted imaging at 3 and 7 Tesla. *Magn Reson Med*. 2015;74:136–149.
40. Ott M, Blaimer M, Grodzki DM, et al. Acoustic-noise-optimized diffusion-weighted imaging. *MAGMA*. 2015;28:511–521.
41. Fritz J, Fritz B, Zhang J, et al. Simultaneous multislice accelerated turbo spin echo magnetic resonance imaging: comparison and combination with in-plane parallel imaging acceleration for high-resolution magnetic resonance imaging of the knee. *Invest Radiol*. 2017;52:529–537.